Aortic Shape Space Geometry

Kameel Khabaz[1], Seth Sankary[1], Karen Yuan[1], Joseph Pugar[2], Sanjeev Dhara[1], Junsung Kim[1], Janet Kang[1], Nhung Nguyen[1], Kathleen Cao[1], Nicole Pierce[1], CJ Lee[3], Ross Milner[1], Gordon Kindlmann[4] and Luka Pocivavsek[1*]

[1]Department of Surgery, The University of Chicago, 5841 S. Maryland Drive, Chicago, 60637, IL, USA.
[2]Department of Material Science, Carnegie Mellon University, Shadyside, Pittsburgh, 15212, PA, USA.
[3]Department of Surgery, NorthShore University Healthcare System, Case Drive, Evanston, 60637, IL, USA.
[4]Department of Computer Science, The University of Chicago, 5730 S. Ellis Ave., Chicago, 60637, IL, USA.

*Corresponding author(s). E-mail(s): lpocivavsek@bsd.uchicago.edu;

Abstract

Aortic disease management depends on aortic anatomy. For decades, maximum aortic diameter has served as the primary parameter of aortic geometry. Size-alone ignores the complex changes in shape occurring during aortic disease progression. We show that a wide spectrum of aortic shapes are all geometrically equivalent to a generalized cylinder. Consequently, aortic size is characterized by a universal scaling law dependent only on cylindrical cross-sectional length $\boldsymbol{\ell}$, irrespective of how $\boldsymbol{\ell}$ is measured. Aortic shape is shown to be topologically invariant; as such, changes in shape are quantified by the variance of integrated Gaussian curvature, $\boldsymbol{\delta K}$, across aortic surfaces. Projecting over three-hundred aortas into our normalized two-dimensional feature $(\widetilde{\boldsymbol{\delta K}}, \tilde{\boldsymbol{\ell}}^{-1})$-space, we discover that aortic morphology evolves with a power-law like behavior with shape preserving growth defining normal aortas and rapidly fluctuating shapes the hallmark of aortic disease. The magnitude of $\widetilde{\boldsymbol{\delta K}}$ strong predicts the success of aortic surgery.

Keywords: aorta, differential geometry, shape, classification

Surgery is anatomy, and anatomy is geometry. Figure 1 shows eight representative aortas along the normal-to-diseased axis. Decision making in modern aortic surgery hinges on parameterizing aortic anatomy using only its maximum diameter [1–3]. However, surgeons appreciate that size alone is an inadequate descriptor of aortic anatomy [3–6]. Since the pioneering days of DeBakey diseased thoracic aortas have been described as 'torturous', 'globular', 'U-shaped', 'dilated', and 'idiosyncratically varying' [7, 8]. These qualitative descriptors underpin the complex changes in shape accompanying aortic disease and its morphologic evolution. Clinically, the need for a mathematical definition of aortic shape is driven by the known problems of using size alone in decision making for various aortic pathologies including coarctations [9], aneurysms [5, 10–13], and aortic dissections [14, 15].

Modern cross-sectional imaging provides detailed three-dimensional aortic reconstructions that can be parameterized into two-dimensional surfaces, see figure 1. Locally the geometry of any surface is defined by its principle curvatures, k_1 and k_2. Specific measures of aortic shape have focused on functions of mean, $\kappa_m = (k_1 + k_2)/2$, or Gaussian, $\kappa_g = k_1 k_2$, curvatures [10, 11], cross-sectional deviations termed eccentricity [14], and calculations on Elastica-like reductions of the aortic surface to space curves or centerlines, leading to measures of centerline tortuosity [15], centerline curvature [16], and centerline bending [17]. Despite these efforts, a mathematically robust and reproducible definition of aortic shape that could enter clinical guidelines or be used for patient classification using modern machine learning algorithems does not exist.

Current methods suffer from spatial over reduction and convolution of shape-size information. Centerline calculations loose information when the aortic surface deforms heterogeneously and non-uniformly [18]. κ_g is the dominant shape function and plays a pivotal role in differential geometry [19]. By itself, κ_g convolutes shape and size; current approaches fail to correctly normalize out the role of size leaving ill defined measures of shape [10, 11]. We solve this problem by performing a Gauss mapping of all normal vectors on a given aortic surface to the unit sphere (see figure 1 and supplemental methods for details). Computationally, the Gauss map is equivalent to calculating the total curvature by integrating κ_g over a given area of the aortic surface: $K = \iint_A \kappa_{\mathrm{g}} dA$ [18–20].

An ideal geometric feature space to track aortic morphogenesis has independent axes for size and shape. It mathematically captures the two regimes apparent in figure 1: a region of normal morphogenesis with shape preserving growth and a region of disease evolution where growth is accompanied by large changes in shape. Our data set contains three-hundred and two aortic segmentations spanning from a healthy 3-year old child to an aneurysmal type B aortic dissection in a 92-year old (see supplemental section 1.1 for full demographics). As noted, maximum aortic diameter, $2R_m$, is the preferred measure of aortic size used clinically. Given the known problems with maximum diameter, a growing literature is studying higher dimensional size parameterizations such as total aortic area, A_T, and aortic volume, V [22, 23]. Even with size, there is a lack of consensus as to the appropriate parameterization.

Geometrically normal and diseased aortas are generalized bent cylinders defined by two length scales: cross-sectional extent ℓ and axial length $\mathcal{L}$. Parameterizing each

aorta along the centerline, the cross-sectional lengths define the distribution of ℓ. Multiple values can be used to represent this distribution: mean aortic radius ($\langle R \rangle$), median aortic radius ($\widetilde{R_2}$), and the distribution maximum value ($2R_m$) are all valid. Furthermore, ℓ can be calculated directly from surface curvatures. The mean Frobenious norm of $\mathbb{S}_i$, the per-vertex aortic shape operator, is the mean inverse linearized aortic Casorati curvature, $\langle C^{1/2} \rangle^{-1}$, a measure of size [24–26].

In Figure 2 Ia., we plot each measure of ℓ versus maximum diameter; the data all collapse onto lines with slope 1, proving the equivalency of the different length scales across all sizes and disease states. We also plot $\sqrt{A_T}$ and $V^{1/3}$. These scalings also collapse onto lines, proving that globally all aortas are truly generalized cylinders with aortic area and volume scaling as $A_T \sim 2\pi c \ell^2$ and $V \sim \pi c \ell^3$, where we used the reparameterization $\mathcal{L} \sim c\ell$. The proportionality constant $c \sim 15$ can be obtained from the linear fits and independently verified by defining $\mathcal{L}$ as the centerline length L of each segmentation and inverting the reparameterization (see supplemental Figure S7).

Normalization with the above pre-factors collapses all size measures onto a single master line (Figure 2 Ib.); irrespective of how much aortic surfaces distort from one person to another by growing, stretching, twisting, or bending, they globally retain a generalized cylindrical geometry concerning their overall area and volume. Furthermore, because of this invariant global geometry, the parametrization of size is dependent only on the single length scale ℓ. This analysis shows that no additional information exists with higher dimensional measurements of size, moreover all consistently applied measurements of ℓ are equivalent. This universal scaling provides the quantitative basis behind the incredible utility of maximum diameter throughout the decades of aortic management and further motivates the study of shape [6].

Figure 1 outlines the workflow of calculating the distribution of K over each aortic surface (see supplemental methods). Figure 2 II plots $\sum K$ as a function of normalized inverse size $\tilde{\ell}^{-1}$. All aortas fall on a line just above $K = 0$ and cluster with the red stars and diamonds, which are perfect tori and cylinders, respectively. By the Gauss-Bonnet theorem, aortic topologic invariance implies that as aortas deform be it through normal growth or pathology every increase in K in some region must be balanced by a proportional decrease elsewhere on the aortic surface [18–20]. Therefore, the distribution of K across the aortic surface holds information about shape. Since ΣK is constant, the variance $\delta K = \langle K^2 \rangle - \langle K \rangle^2$ captures the balance of positive and negative curvature regions across the surface and is a measure of shape. Figure 2 III. plots $\widetilde{\delta K} = \delta K / \min|\delta K|$ versus $\tilde{\ell}^{-1}$. Normal aortas (black circles) have a nearly constant $\widetilde{\delta K}$ from the smallest aorta in a 3-year old child to the largest in a 92-year old. $\widetilde{\delta K} \sim$ constant is thus the mathematical signature of shape preserving growth seen in normal aortas. Following the yellow symbols, corresponding to the representative segmentations in Figure 1, allows a direct visual comparison between the development of pathology and the divergence of $\widetilde{\delta K}$. The data projected in the $(\widetilde{\delta K}, \tilde{\ell}^{-1})$-space fit to a power law $\widetilde{\delta K} = 2(1/\tilde{\ell})^{-4} + 1$. The existence of a power law behavior is further supported by the power-law probability distribution of δK (see supplemental Figure S8).

No general theory exists on the meaning of δK divergence. However in soft matter systems such as spherical vesicles, where size weakly changes, and in dynamical systems rapid fluctuations of κ_g have been linked to so-called 'topologic catastrophes' indicative of approaching instabilities [26, 27]. In vesicles, the instability manifests as the physical breakup of the system [25, 26]: budding, fusion, or rupture; in dynamic systems, the topologic catastrophe indicates the development of turbulence [27]. While we do not inherently study aortic stability as it relates to clinical rupture in this paper, aortas appearing at high δK are clinically classified by size and qualitative appearance as high risk. It is therefor interesting to conjecture that divergence in the $(\widetilde{\delta K}, \tilde{\ell}^{-1})$-space is a sign of aortic topologic instability and an indicator of aortic fragility.

To further study δK as an aortic descriptor, machine learning (ML) methods were used to quantify its utility as a patient classification feature among other shape measurements. Our cohort includes two diseased patient populations which are classified based upon their clinical outcomes with surgery using thoracic endovascular aortic repair, TEVAR, (dark and light gray symbols in Figure 2 III.). ML can be used to build predictive classification models from sets of training data by identifying and leveraging underlying trends to make predictions and thus can be built to predict outcomes from size and shape measurements. Using a logistic regression model, we show that δK significantly outperforms all available measures of shape in classifying between non-pathologic aortas, aortas with successful TEVAR, and aortas with failed TEVAR (supplemental Figure S14 Ib. and Table S3). This result can be interpreted as δK being the best second parameter to add to ℓ in creating a two-dimensional shape$\times$size space from which the most accurate classification occurs. The analysis also shows statistical parity between all measures of size (supplemental Figure S14 Ia.), independently validating our geometric analysis in Figure 2. Furthermore, a single variable linear space defined by maximum diameter, while widely used, is inherently problematic because a critical point between closely spaced and overlapping normally distributed populations is very sensitive to the available data (supplemental Figure S15 I.); a well-known problem in maximum diameter based criteria is the bias against smaller statured female patients because of the heavily male-waited population-based statistics on aortic sizes [68, 69]. Projection into $(\delta K, \tilde{\ell}^{-1})$-space provides two independent variables that show a natural division of the data as it transitions from size to shape-dominated behavior as seen in supplemental Figure S15 II. Classification is significantly more accurate in the $(\delta K, \tilde{\ell}^{-1})$-space compared to the R_m-space; moreover, the former is far more robust and less sensitive to data variability. Lastly, while the ML model's learned decision boundaries (i.e., classification thresholds) are limited in their universal interpretation, they do offer an unbiased source of evidence that one, introducing δK improves class separation and classification accuracy most among other shape factors and two, an underlying transition between successful and failed TEVAR may be primarily governed by aortic shape factors.

This paper presents a solution to the decades old problem of identifying a second quantifiable anatomic feature in aortic classification to supplement maximum aortic diameter. The stability and success of novel endovascular surgical solutions to complex aortic pathologies such as dissections and aneurysms is being severely curtailed

by the inability to correctly characterize patient anatomy form imaging data [3–6]. Future endovascular technology development and surgery personalization to given patient anatomies is dependent on integrating aortic size and shape. Discovering the topologic invariance of aortic shapes, allows us to use Gauss mappings to identify a feature purely dependent on shape. $(\delta K, \tilde{\ell}^{-1})$-space projection is broadly applicable to other aortic pathologies including abdominal and ascending aneurysms. Moreover, because the methodology is based on a general geometric and topologic foundation, it can be extended to other problems of growing shapes in medical imaging such as tumor classification [28], solid organ trauma [29], cerebral aneurysms [30], and left ventricular failure [31].

Acknowledgments: We acknowledge the support of the National Institutes of Health, NHLBI, R01HL159205. We are grateful to Enrique Cerda, Efi Efrati, Haim Diamant, and Thomas Witten for careful reading of the text and detailed comments.

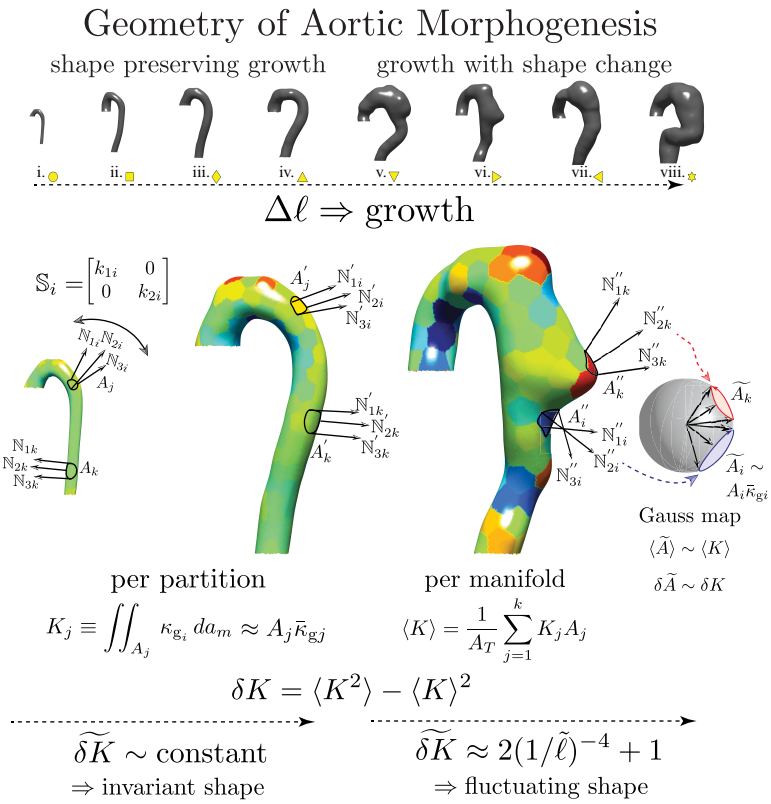

Fig. 1 Eight representative aortas along the normal-to-diseased axis: ranging from a 3 year-old child (i.) to healthy adults (ii. and iii.); iv. through viii. are from type B aortic dissection (TBAD) patients at varying degrees of aneurysmal degeneration. Two clinical regimes exist: shape preserving growth (i.→iii.) and growth with shape changes (iv.→viii.). Aortas are generalized bent cylinders; as such, changes in size are defined by following a single length scale: cross-sectional extent ℓ, which is clinically defined as maximum diameter [6]. By mapping the aortic surface to the unit sphere (Gauss map [18]), we have an independent measure of shape. All computations are performed in an extrinsic geometric framework using surface normals, $\mathbb{N}_i$. The mesh density is set by the resolution of the CT scans and is constant for all aortas. The per-vertex shape operator $\mathbb{S}_i$ is calculated using the Rusinkiewicz algorithm [21]. To minimize noise, the aorta is partitioned into multiple patches with area A_j. The local integrated Gaussian curvature K_j is calculated as the product of patch area and mean Gaussian curvature, $\bar{\kappa}_{gj}$, where care is taken that the per-vertex κ_{gi} has small spatial variation within A_j [19] (see Supplemental Methods). K_j is equivalent to the signed patch area $\widetilde{A_j}$ mapped out by the normals projected onto the unit sphere; K_j and $\widetilde{A_j}$ are topologic invariants. We define aortic shape by studying the statistics of the distributions of K_j. The first, $\langle K \rangle$, and second, δK, distribution moments define aortic shape geometry. Figure 2 shows that δK is a powerful variable with which to track aortic shape changes.

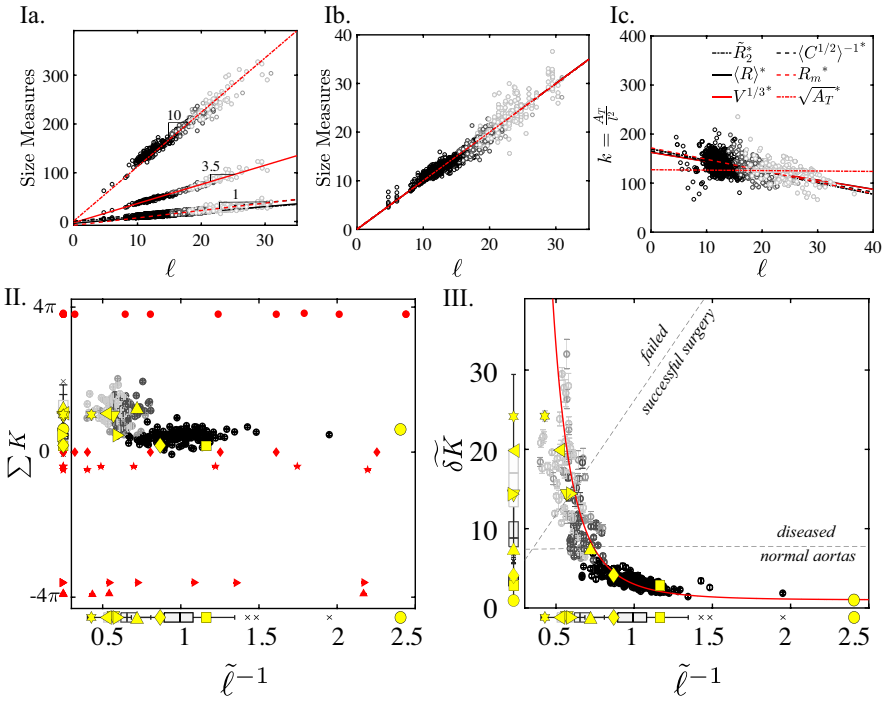

Fig. 2 Aortic size is clinically parameterized by measuring maximum aortic diameter, $2R_m$. Data for three-hundred and two patients, including non-pathologic (black circles) and pathologic (light, failed TEVAR, and dark, successful TEVAR, gray circles) aortas, are plotted. **Ia.** shows that there is mathematical equivalency between multiple one-dimensional parameterizations of aortic size including mean aortic radius ($\langle R\rangle$), median aortic radius ($\widetilde{R_2}$), and mean inverse linearized aortic Casorati curvature, $\langle C^{1/2}\rangle^{-1}$, scale in mm. Furthermore, higher dimensional measures of size, such as aortic area and volume, when dimensionally scaled, $\sqrt{A_T}$ and $V^{1/3}$, are also linear when plotted against ℓ. All size measures can be collapsed onto a single master curve (**Ib.**), proving that irrespective of the degree of aortic shape distortion overall aortic size scales as a generalized curved cylinder parameterizable by a single length scale ℓ. **Ic.** The linear scaling can be used to define $A_j \sim \ell^2$, which sets the number of partitions k used in the Gauss map calculations. **II.** shows the topologic invariance of all aortic shapes and their equivalence to tori (red stars) and cylinders (red diamonds), with $\sum K \approx \langle K\rangle \sim 0$; the yellow symbols correspond to the specific shapes shown in Figure 1. The x-axis is normalized inverse size measure $\tilde{\ell}^{-1} = \ell^{-1}/\langle\ell\rangle_{norm}^{-1}$, where $\langle\ell\rangle_{norm}$ is the mean of the normal aortas. Red circles correspond to perfect spheres of varying size; pseudospheres and catenoids are depicted as red rightward-pointing triangles and upward-pointing triangles, respectively. For these constant positive and negative κ_g surfaces, our computed $\sum K$ agrees with analytical values, serving as a validation of our computational methodology. **III.** shows the optimal two-dimensional aortic geometric feature space with independent axes for size ($\tilde{\ell}^{-1}$) and shape ($\widetilde{\delta K}$). The solid red line is a best fit to the data showing a power-law like behavior $\widetilde{\delta K} = 2(1/\tilde{\ell})^{-4} + 1$, which is further supported by the power-law probability distribution of δK (see supplemental figure S7). The aortas strongly separate into shape invariant (normal) and shape fluctuating (diseased) populations. Furthermore, this feature space allows us to define decision boundaries (dashed lines) which not only separate normal from diseased, but also correctly classify diseased patients based upon success of TEVAR (see figure S14.

References

[1] Paruchuri V, Salhab KF, Kuzmik G, et al. *Aortic Size Distribution in the General Population: Explaining the Size Paradox in Aortic Dissection.* Cardiology. 2015;131(4):265-272. doi:10.1159/000381281

[2] Nauta FJ, Trimarchi S, Kamman AV, et al. *Update in the management of type B aortic dissection.* Vasc Med. 2016;21(3):251-263. doi:10.1177/1358863X16642318

[3] T.E. MacGillivray, T.G. Gleason, H.J. Patel et al. *The Society of Thoracic Surgeons/American Association for Thoracic Surgery Clinical Practice Guidelines on the Management of Type B Aortic Dissection* Ann. Thorac. Surg, 2021; XX-XX

[4] D. Fleischmann et. al. *Imaging and Surveillance of Chronic Aortic Dissection: A Scientific Statement from the American Heart Association* Circulation Cardiovascular Imaging, 2022. **15**: e000075.

[5] Liang L, M. Liu, C. Martin, J.A. Elefteriades, and W. Sun. *A Machine Learning Approach to Investigate the Relationship Between Shape Features and Numerically Predicted Risk of Ascending Aortic Aneurysm.* Biomech Model Mechaniobiol 2017; (16):1519-1533. doi 10.1007/s10237-017-0903-9.

[6] Spinelli, D., F. Benedetto, R. Donato, G. Piffaretti, M.M. Marrocco-Trischitta, H.J. Patel, K.A. Eagle, and S. Trimarchi. *Current Evidence in the Predictors of Aortic Growth and Events in Acute Type B Aortic Dissection.* J. Vasc. Surg. 2018; 68: 1925-1935.

[7] DeBakey, M.E., D.A. Cooley, and O. Creech, *Surgical Considerations of Dissecting Aneurysm of the Aorta* Annals of Surgery, 1955. **142** (4): p. 586-610.

[8] Dake, M.D., D.C. Milber, C.P. Semba, R.S. Mitchell, P.J. Walker, and R.P. Liddell. *Transluminal Placement of Endovascular Stent-Grafts for the Treatment of Descending Thoracic Aortic Aneurysms* The New England Journal of Medicine, 1994. **331** (26): p. 1729-1734.

[9] Bruse JL, Khushnood A, McLeod K, et al. *How successful is successful? Aortic arch shape after successful aortic coarctation repair correlates with left ventricular function.* J Thorac Cardiovasc Surg. 2017;153(2):418-427. doi:10.1016/j.jtcvs.2016.09.018

[10] Shum J, Xu A, Chatnuntawech I, Finol EA. *A Framework for the Automatic Generation of Surface Topologies for Abdominal Aortic Aneurysm Models.* Ann Biomed Eng. 2011;39(1):249-259. doi:10.1007/s10439-010-0165-5

[11] Lee K, Zhu J, Shum J, et al. *Surface Curvature as a Classifier of Abdominal Aortic Aneurysms: A Comparative Analysis.* Ann Biomed Eng. 2013;41(3):562-576. doi:10.1007/s10439-012-0691-4

[12] Urrutia J, Roy A, Raut SS, Antón R, Muluk SC, Finol EA. *Geometric surrogates of abdominal aortic aneurysm wall mechanics.* Med Eng Phys. 2018;59:43-49. doi:10.1016/j.medengphy.2018.06.007.

[13] Casciaro, ME, D. Craiem, G. Chironi, S. Graf, L. Macron, E. Mousseaux, A. Simon, and R.L. Armentano. *Identifying the Principal Modes of Variation in Human Thoracic Aorta Morphology.* J. Thorac Imaging. 2014; (29):224-232.

[14] Bondesson J, Suh GY, Marks N, Dake MD, Lee JT, Cheng CP. *Influence of thoracic endovascular aortic repair on true lumen helical morphology for Stanford type B dissections.* J Vasc Surg. 2021;74(5):1499-1507.e1. doi:10.1016/j.jvs.2021.04.029

[15] Chen CK, Liang IP, Chang HT, et al. *Impact on outcomes by measuring tortuosity with reporting standards for thoracic endovascular aortic repair.* J Vasc Surg. 2014;60(4):937-944. doi:10.1016/j.jvs.2014.04.008

[16] Giannoglou, G, G. Giannakoulas, J. Soulis, Y. Chatzizisis, T. Perdikides, N. Melas, G. Parcharidis, and G. Louridas. *Predicting the Risk of Rupture of Abdominal Aortic Aneurysms by Utilizing Various Geometrical Parameters: Revisiting the Diameter Criterion.* Angiology. 2006;57(4):487-494. doi:10.1177/0003319706290741

[17] Li D, Peng L, Wang Y, Zhao J, Yuan D, Zheng T. *Predictor of false lumen thrombosis after thoracic endovascular aortic repair for type B dissection.* J Thorac Cardiovasc Surg. 2020;160(2):360-367. doi:10.1016/j.jtcvs.2019.07.091

[18] Tristan Needham *Visual Differential Geometry and Forms - a mathematical drama in five acts* Princeton University Press, Princeton, NJ, 2021.

[19] Barrett O'Neill *Elementary Differential Geometry, 2nd ed* Academic Press, Burlington, MA, 2006.

[20] Jan. J. Koenderink *Solid Shape* The MIT Press, Cambridge, Massachustts, 1990.

[21] S. Rusinkiewicz *Estimating Cruvatures and Their Derivatives on Triangle Meshes.* In Proceedings. 2nd International Symposium on 3D Data Processing, Visualization and Transmission, 2004. 3DPVT 2004., pages 486–493, September 2004.

[22] Song JM, Kim SD, Kim JH, et al. *Long-Term Predictors of Descending Aorta Aneurysmal Change in Patients With Aortic Dissection.* J Am Coll Cardiol. 2007;50(8):799-804. doi:10.1016/j.jacc.2007.03.064

[23] Kim TH, Ko YG, Woo Kwon S, et al. *Large False Lumen Area Is a Predictor of Failed False Lumen Volume Reduction After Stent-Graft Repair in Type B Aortic Dissection.* J Endovasc Ther. 2014;21(5):697-706. doi:10.1583/14-4671MR.1

[24] Koenderink, J., van Doorn, A., and Wagemans, J. *Local Solid Shape.* i-Perception, 2015. **6** (5), 1-15.

[25] Aguilar Gutierrez, O.F. and A.D. Rey. *Extracting Shape from Curvature Evolution in Moving Surfaces.* Soft Matter, 2018. **14**, 1465.

[26] McClure, J.E., S. Berg, and R.T. Armstrong. *Geometric Evolution as a Source of Discontinuous Behavior in Soft Condensed Matter.* arXiv:1906:04073, 2019

[27] Marco Pettini *Geometry and Topology in Hamiltonian Dynamics and Statistical Mechanics* Springer, New York, NY, 2007.

[28] Limkin, JL, Reuze, S., Carre, A., Sun, R., Schernberg, A., Alexis, A., Deutsch, E., Ferte, C., and C. Robert. *The Complexity of Tumor Shape, Spiculatedness, Correlates with Tumor Radiomic Shape Features.* Scientific Reports. 2019; (9):4329.

[29] Farzaneh, N., Stein, E.B., Soroushmehr, R., Gryak, J., and K. Najarian. *A Deep Learning Framework for Automated Detection and Quantitative Assessment of Livier Trauma.* BMC Medical Imaging. 2022; (22):39.

[30] Ma B, Harbaugh RE, Raghavan ML. *Three-Dimensional Geometrical Characterization of Cerebral Aneurysms.* Ann Biomed Eng. 2004;32(2):264-273. doi:10.1023/B:ABME.0000012746.31343.92

[31] Medvedovsky, D., Maffessanti, F. Weinert, L., Tehrani, D.M., Narang, A., Addetia, K., Mediratta, A., Besser, S.A., Maor, E., Patel, A.R., Spencer, K.T., Mor-Avi, V., R.M. Lang. *2D and 3D Echocardiography-Derived Indices of Left Ventricular Function and Shape: Relationship With Mortality.* JACC: Cardiovascular Imaging. 2018; (11):1569-1579.